International Journal of
INTELLIGENT SYSTEMS AND APPLICATIONS IN ENGINEERING
ISSN:2147-6799 www.ijisae.org Original Research Paper

# Closed Loop PI Control of PV Tied Grid System with Multi-Carrier PWM Based Modular 5-Level Converter

**K. Praveena[1,*], Katragadda Swarnasri[2]**

**Submitted:** 22/07/2022 **Accepted:** 25/09/2022

***Abstract:*** As the contribution of PV in the area of power production is significantly high in the recent period, it is preferred in various applications. In this present study, a control scheme is proposed for tracking the maximum power from each individual PV module. Due to the changes in temperature, the output of PV gets oscillated and fails to provide constant DC voltage. A Modular 5-level converter (M5LC) is employed, which converts the fluctuating voltage of PV module into a constant value. This DC-DC converter is controlled by the aid of multi-carrier PWM technique. By implementing PI controller, the reference signal is generated and analogized with the carrier signals of MCPWM technique for generating the gating sequence to control the M5LC. The converter's DC output voltage is fed to the 3Φ VSI, which converts the DC into AC voltage. The gating pulses of the inverter is generated with help of PI controller, through which the grid synchronization is achieved and the THD is minimized. The proposed control method is validated through MATLAB simulation.

***Keywords:*** *PV module, Modular 5-level Converter, Half bridge sub-module, Multi-carrier PWM technique, PI controller, Grid synchronization***.**

## 1. Introduction

In power generation, the role of PV has significantly improved in recent years through the technological advancements, because of which the cost of power electronic devices is minimized. Due to the beneficial factors like simple installation, less maintenance cost and minimum fuel cost, the use of PV based power production is rapidly increasing. The main purposes of integrating the grid with the PV system are to decrease the cost and increase the efficiency. To accomplish these objectives, a single-stage DC-AC power converter system is utilized [1-3]. In the grid tied PV inverters, the efficiency and price are the important factors. These inverters have linked the PV array with the grid connected low-frequency isolation transformer. As these transformers are bulky and costly, additional losses are produced, which have been overcome by the high-frequency isolation transformer [4]. The MPPT techniques are utilized to extricate the maximum power from PV array [5].

As the PV output is fluctuating, it fails to provide constant DC voltage and thus different kinds of DC-DC converters are generally utilized to improve the PV voltage [6]. To step up the voltage, a boost converter is utilized, which has delivered sudden rise in the input current and increased the power losses during the period of switching [7]. The above mentioned drawback is eradicated with the utilization of Buck-Boost converter, which has the capacity of operating in both buck and boost modes. The voltage gain of this converter is not sufficient for the power generation of PV module [8]. With the utilization of CUK converter, the DC-link potential is retained by the incorporated voltage control but this voltage fails to meet the necessity of grid voltage [9]. The SEPIC converter is utilized, which minimizes the efficiency of the converter [10]. Thus, a Modular Multilevel Converter (MMC) is presented in the proposed work to overcome all the above stated problems.

Different PWM methods are utilized to regulate the output potential of MMC. The phase shifted pulse width amplitude modulation (PS-PWAM) method is utilized to minimalize the switching loss and to boost up the voltage gain. However, the implementation of this technique is highly complex [11, 12]. With the utilization of selective harmonic elimination and selective harmonic mitigation PWM (SHEPWM and SHMPWM) methods, the number of voltage levels are increased, which leads to difficulties in calculation [13, 14]. In this study, the Multicarrier PWM techniques are utilized to regulate the MMC as it has the benefit of easy and simple implementation. Two

[1] *Department of EEE, Acharya Nagarjuna University, Guntur, Andhra Pradesh, India.*
[2] *Department of EEE, R.V.R & J.C College of Engineering, Guntur, India.*
[*] *Corresponding Author Email: praveena.eee123@gmail.com*

categories of MMC topologies like two-level submodule and multilevel submodule are given importance, among which the two-level submodule involves half-bridge submodule (HBSM) and full-bridge submodule (FBSM) [15]. In this study, the PI controller is employed to achieve grid synchronization by controlling the VSI.

The PV integrated grid system with Multi-Carrier PWM assisted M5LC based PI controller is presented in this study. The output of PV is improved with the help of M5LC and the output of converter is controlled by using MCPWM technique. The PI controller has been instigated to control the switches of converter and inverter to achieve grid synchronization. The detailed description about the PV panel, MMC, MCPWM technique, PI controller, 3Φ VSI grid synchronization and LC filter design are given below.

## 2. Proposed Control Scheme

As the DC output voltage of PV is derived with fluctuations, it is essential to enhance the voltage by using an appropriate DC-DC converter. Due to its easy scalability and high modularity, a M5LC is chosen in this study, which improves the permanence of the system. The schematic illustration of PV integrated grid scheme with M5LC control scheme is represented in Fig. 1.

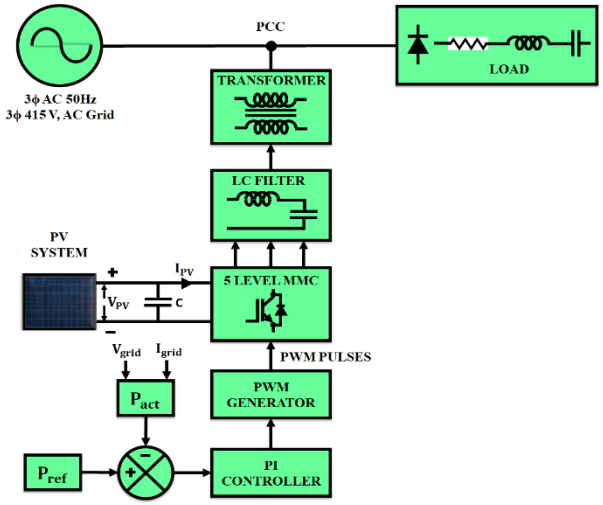


**Fig. 1.** Schematic representation of control scheme

To retain the DC link voltage as constant, the M5LC is controlled with the assistance of multicarrier PWM techniques. This output is fed to the grid through a 3Φ VSI, which converts the DC into AC voltage. The reference signal is generated and analogized with the carrier signals of multicarrier PWM technique by the utilization of PI controller, through which the grid synchronization is achieved and THD is reduced.

## 3. Modelling of Proposed System

### 3.1. Modelling of PV panel

Solar panels absorb and convert the sunlight into electric power. When solar cells are linked in series and parallel, a PV module is created, which converts the photon energy into electricity. The circuit layout of PV module is illustrated in Fig. 2.

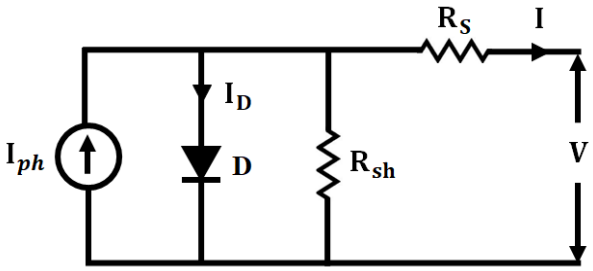


**Fig. 2.** Circuit layout of PV module

The PV system is modelled as an ideal PV cell with a current source $(I_{ph})$, which is shunt connected to the diode. When applying the KCL in the above circuit, it is expressed as,

$$I = I_{ph} - I_d \tag{1}$$

The diode current $(I_d)$ is expressed as,

$$I_d = I_s \left[ exp\left(\frac{qV_{OC}}{N_S K A T_O}\right) - 1 \right] \tag{2}$$

Substitute equation (2) in (1)

$$I = I_{ph} - I_s \left[ exp\left(\frac{qV_{OC}}{N_S K A T_O}\right) - 1 \right] \tag{3}$$

Solar cell provides good approximation for the generation of photon current, which is directly proportional to the intensity and solar irradiance.

For modelling the PV system in real case, the effect of series resistance $R_s$ is applied in equation (3), which is expressed as,

$$I = I_{ph} - I_s \left[ exp\left(\frac{q(V+IR_S)}{N_S K A T_O}\right) - 1 \right] \tag{4}$$

The output current $(I)$ is changed when the PV cells are interfaced in a series–parallel manner, which is expressed as,

$$I = N_p * I_{ph} - N_p * I_s \left[ exp\left(\frac{q(V+IR_S)}{N_S K A T_O}\right) - 1 \right] \tag{5}$$

Where,

$$I_{ph} = [I_{SC} + K_i(T_o - T_r)] * \frac{G}{G_{ref}} \tag{6}$$

The voltage output of the PV is provided to the M5LC to retain the PV voltage as constant.

### 3.2. Modelling of Modular Multilevel Converter (MMC)

The MMC based HBSM has the modular characteristics features for giving higher quality output potential and providing harmonics free current waveforms. The converter's operation depends on the switching frequency of each individual SM of the converter. The

MMC's each phase legs are made up of upper and lower arms, which contain multiple SM. The MMC with $(2N + 1)$ voltage levels are created by linking the PV array with a capacitor and HBSM. As 5 level MMC is employed in this work, every phase has two SM. The schematic structure of MMC is illustrated in Fig. 3.

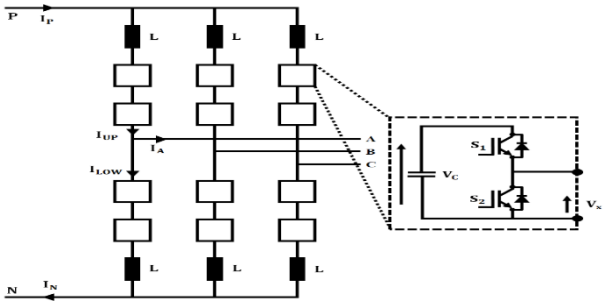


**Fig. 3**. Schematic structure of MMC

To produce the multilevel waveform in the output, the required voltage of the individual SM has to be retained. If a SM is switched $ON\ or\ OFF$, the voltage levels in the output of converter has been increased. The number of SMs, which are linked in the phase-leg is not constant in an MMC. The sum of potentials in the phase-leg is changed not only by the changes in the voltage across capacitance but also by the load current. The $2N + 1$ levels in the converter's output generates a waveforms with lower harmonic distortion. The arm voltage is expressed as,

$$V_{arm} = \sum_{i=1}^{N} S_{SM}.V_{C,SM} + L_{arm}\frac{di_{arm}}{dt} \quad (7)$$

The M5LC's output is attained by controlling the multi-carrier PWM technique through the generation of gating pulses.

### 3.3. Modeling of Multicarrier PWM (MCPWM) Technique

The M5LC and 3Φ VSI are controlled with the aid of MCPWM, which lowers the total harmonic distortion of output voltage**.** In order to produce the switching pulses for the M5LC, the reference signal (single sine wave) is analogized with the carrier signal (triangular wave). By using the larger number of carriers, the sine PWM technique is applied in the multi-level converter modules. It needs $(n - 1)$ carrier waves for a $n$ level converter. It is categorized as Level Shifted PWM (LSPWM) and Phase Shifted PWM (PSPWM). In former, the carrier signals are vertically arranged whereas in latter, the carrier signals are horizontally arranged. The following equations calculate the values of amplitude and time.

$$A_{k+1} = \sum_{k=1}^{(n-1)/2} A_k - \frac{4A_1}{n-1} \quad (8)$$

$$A_{k+1} = \sum_{k=(n+1)/2}^{n} A_k + \frac{4A_1}{n-1} \quad (9)$$

$$T_k = \frac{k-1}{(n-1)f} \quad (10)$$

Where $k$ indicates the positive integer number.

#### *3.3.1 Generation of Multicarrier signals*

The gating pulses for the switches are produced by analogizing the reference signal with the carrier signals. If $A_{ref}$ denotes reference signal's peak to peak amplitude and $A_c$ denotes carrier signal's peak to peak amplitude, then the amplitude modulation index, $m_a$ is,

$$m_a = \frac{A_{ref}}{n\,A_c} \quad (11)$$

The frequency modulation index, $m_f$ is defined as the ratio of required frequency of carrier signals, $f_c$ to the frequency of modulating signal, $f_m$.

$$m_f = \frac{f_c}{f_m} \quad (12)$$

The pulse generation control diagram is illustrated in Fig. 4. At every instant, the reference signal is analogized with the carrier signals to produce pulses for the switches. If the reference signal is larger than zero with the positive carriers, the pulse generation is '1' *or* '0' and if the reference signal is larger than zero with the negative carriers, the pulse generation is ' $-1$' *or* '0'.

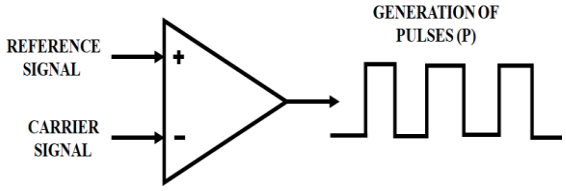


**Fig. 4.** Pulse generation control diagram

The equation of pulse generation is expressed as,

$$P^{+} = \begin{cases} 1, & if\ M \geq C_r^{+} \\ 0, & if\ M < C_r^{+} \end{cases} \quad (13)$$

$$P^{-} = \begin{cases} -1, & if\ M \geq C_r^{-} \\ 0, & if\ M < C_r^{-} \end{cases} \quad (14)$$

With the aid of multicarrier PWM technique, the pulses are generated to control the switches of M5LC.

### 3.4. Modeling of PI controller

To achieve grid synchronization in PV integrated grid system, the PI controller is employed for producing the reference signal. This reference signal are analogized with the carrier signals of MCPWM technique, through which the gating sequence of 3Φ VSI are generated to control the inverter switches. The Pi controller's control block representation is portrayed in Fig. 5.

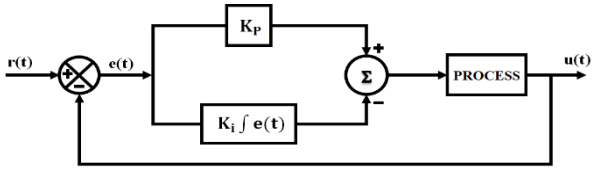


**Fig. 5.** Control block representation of PI controller

The PI controller gives the error signal as output. The combination of two different controllers eliminates the drawbacks of using individual controllers. The PI controller generates an output signal, $u(t)$, which comprises two levels like input signal, $e(t)$ and integral of input signal, $e(t)$. The steady state error has been decreased by this controller. The PI controller's output signal is proportional to the error signals, which is expressed as,

$$u(t) \propto [e(t) + \int e(t)dt] \tag{15}$$

$$u(t) = K_p e(t) + K_i \int e(t)dt \tag{16}$$

Where the proportional gain is denoted as $K_p = -\omega_1 sin\theta / A_1$ and the integral gain is denoted as $K_i = cos\ \theta / A_1$. The PI controller's transfer function is specified as,

$$G_c(s) = U(s)/E(s) = K_p + K_i/s \tag{17}$$

### 3.5. Modeling of Three phase Grid synchronization

To synchronize the PV with the grid, the output voltage of 5 level MMC's constant DC voltage has to be converted into AC. Thus, a 3Φ VSI is utilized to convert the DC into AC voltage. The structure of 3Φ grid connected VSI is illustrated in Fig. 6.

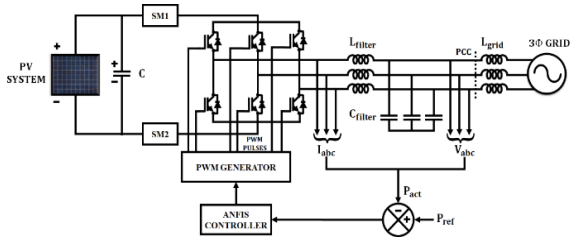


**Fig. 6**. 3Φ Grid connected VSI

To regulate the grid power, PI controller is employed, which generates the gating sequences of 3Φ VSI. For synchronizing the PV with grid, the PCC voltage, frequency and phase angle are required for producing the reference current. For 3Φ systems, the PLL is mounted on the synchronously rotating reference frame, which simplifies the loop filter structure. Because of the nonlinear loads, the grid voltage gets fluctuated, which is eradicated with the aid of SRF-PLL. The SRF-PLL provides precise frequency and phase angle for the estimation of grid voltage. Thus the grid synchronization is attained and the THD is minimized.

### 3.6. Modeling of LC Filter Design

The AC current ripples and the inductance across the inverter are utilized with 5% of phase current at rated power to design the LC filter. With this rule, the grid current is presumed as zero and the voltage across the inductive filter is also equivalent to zero. The voltage across the inductor is expressed as,

$$V_L = V_{inv} - V_g \tag{18}$$

Where $V_L$ indicates the voltage across inductor, $V_{inv}$ indicates the output voltage of inverter and $V_g$ indicates the grid voltage.

As the grid frequency $f_N$ is lesser than the switching frequency $f_s$, the phase voltage depends upon the switching frequency $f_s$,. The inductive filter current's peak-to-peak value is expressed as,

$$\Delta I_{pp} = 2I_{rpm} = \frac{\frac{V_{dc}}{2} - V_{av}}{L_f} . \frac{d_1}{f_s} \tag{19}$$

Where $I_{pp}$ indicates the inductive filter current ripple's peak-to-peak value, $V_{av}$ indicates the inverter's average value of output voltage, $I_{rpm}$ indicates the maximum value of inductive filter, $L_f$ indicates the inductive filter and $d_1$ indicates the duty cycle. During the range $0 < \omega t < \pi$,

$$V_{av}(\omega t) = d_1(\omega t) \frac{V_{dc}}{2} \tag{20}$$

$$d_1(\omega t) = m_a sin(\omega t) \tag{21}$$

Where $m_a$ indicates the modulation index. The value of maximum inductive current ripple, $I_{rpm}$ is expressed as,

$$I_{rpm} = \frac{V_{dc}}{4L_f f_s}[1 - d_1(\omega t)]\, d_1(\omega t) = \frac{V_{dc}}{4L_f f_s}[1 - m_a sin(\omega t)] m_a sin(\omega t) \tag{22}$$

When $m_a = 1$, the maximum value of $I_{rpm}$ is $1/4$ at $\pi/6, 5\pi/6$.

$$L_f = \frac{V_{dc}}{16 f_s \Delta I_{ph(max)}} \tag{23}$$

The variation of maximum power factor shown by the grid is set as 5% when choosing the capacitive filter. The base impedance of complete system, $Z_B$ is determined from the variation in capacitance, which is expressed as,

$$Z_B = \frac{v_G^2}{P_{AV}/3} \tag{24}$$

$$C_B = \frac{1}{\omega_N Z_B} = \frac{1}{2\pi f_N Z_B} \tag{25}$$

Where $v_G$ indicates the rms value of line-to-line voltage, $P_{AV}$ indicates the rated real power and $\omega_N$ indicates the grid frequency.

## 4. Results and Discussions

The PV tied grid system is analyzed in this study, in which the conversion of DC-DC is carried out by the M5LC and the conversion of DC-AC is carried out by 3Φ VSI. The reference signal is generated and analogized with the carrier signals of MCPWM technique by implementing PI controller to regulate the converter. The converter's DC output voltage is fed to the grid through a 3Φ VSI, which converts the DC into AC voltage to attain grid synchronization. The proposed control scheme is simulated trough MATLB software. The specifications of proposed system are represented in Tab. 1.

**Table 1.** Specifications of proposed system

| Specifications | Values |
|---|---|
| Power rating of solar panel | $30KW$ |
| Number of panels | 300 |
| Total number of series cells | 36 |
| Cell Area | $125mm \times 31.25mm$ |
| Temperature Range | $-40\ to\ 85^0\ C$ |
| Maximum Voltage of converter and inverter | $1000\ V$ |
| Operating Voltage of single solar panel | $16.8\ V$ |
| Operating Current of single solar panel | $5.8\ A$ |
| Power rating of single solar panel | $\approx 100W$ |
| LC Filter | $4.5mH/10\mu F$ |
| Switching frequency | $20KHz$ |
| Grid frequency | $50Hz$ |

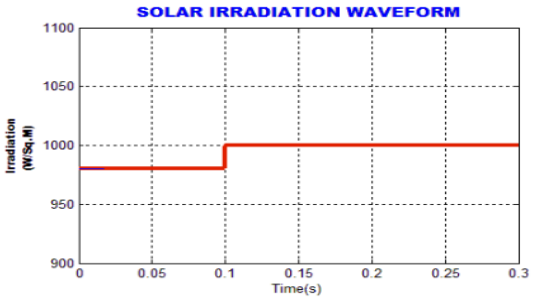


**Fig. 7**. Solar irradiation waveform

The solar irradiation waveform is illustrated in Fig. 7. Initially, the solar irradiation is set at $980\ W/m^2$ between the time of $0\ to\ 0.1\ s$ but after the time of $0.1\ s$, the irradiation is set at $1000\ W/m^2$.

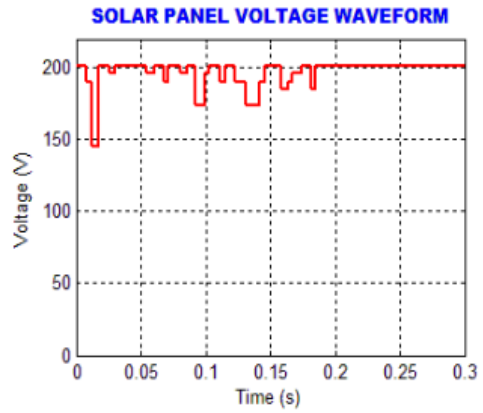


**(a)**

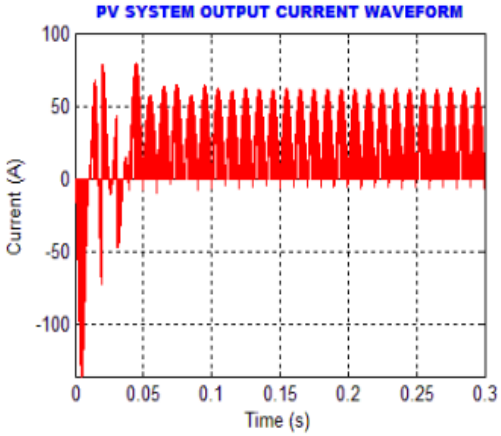


**(b)**

**Fig. 8.** (a) Voltage waveform of PV panel (b) Current waveform of PV panel

The voltage and current waveforms of PV panel are illustrated in Fig. 8 (a) & (b). Due to temperature changes, the output voltage of PV panel is fluctuated in the initial stage, which is maintained as constant after the time of $0.18s$ at the voltage of $200V$. If the PV module's output voltage is varied, the output current of PV gets varied.

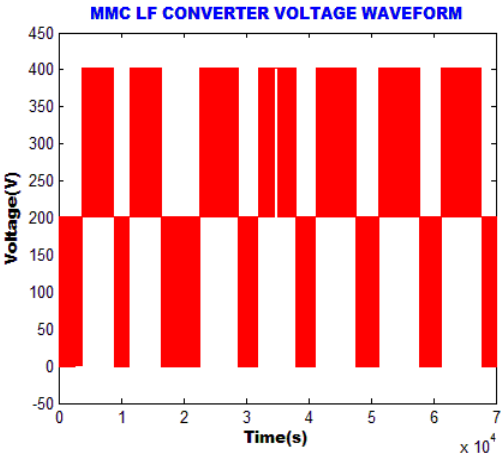


(a)

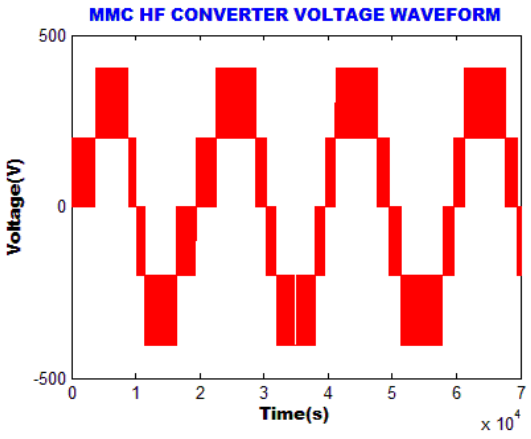


(b)

**Fig. 9**. (a) MMC LF converter voltage waveform (b) MMC HF converter voltage waveform

The voltage waveforms of MMC LF and MMC HF converter are illustrated in Fig. 9 (a) & (b). In MMC LF converter voltage waveform, the voltage is obtained between $0\ to\ 400V$. In MMC HF converter voltage waveform, the voltage is obtained between $0\ to +400V\ and\ 0\ to -400V$, which comprises 5 levels.

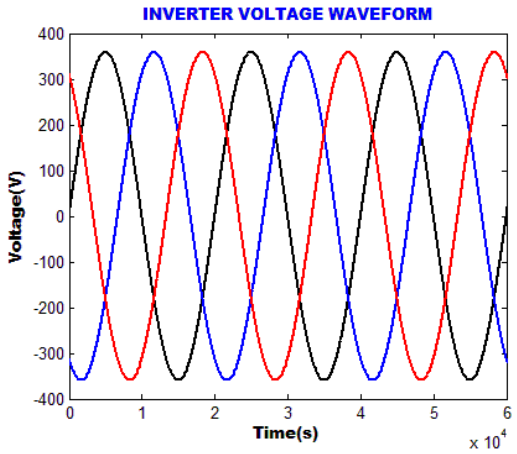


(a)

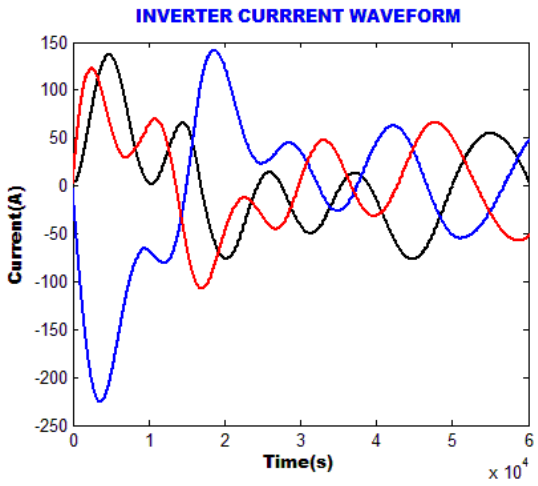


(b)

**Fig. 10.** (a) Voltage waveform of inverter (b) Current waveform of inverter

The voltage and current waveforms of the inverter are illustrated in Fig. 10 (a) & (b). In the inverter current waveform, the harmonics are occurred in the initial stage but after the time of $3 \times 10^{-4}\ s$, the harmonics are eliminated with the working of M5LC, through which the waveform becomes sinusoidal.

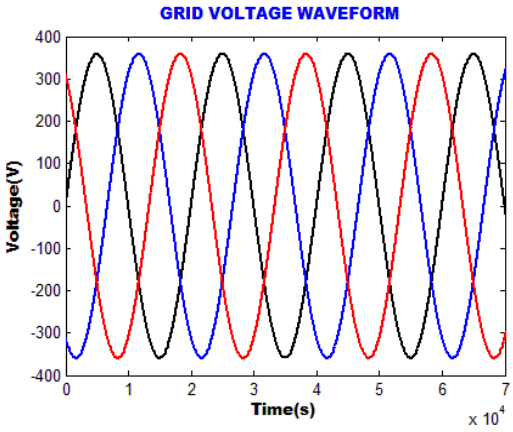


**(a)**

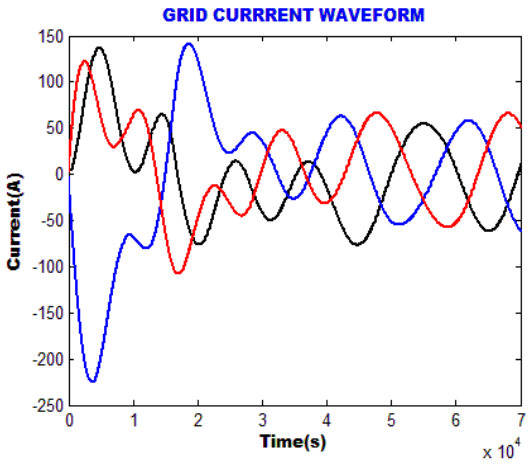


(b)

**Fig. 11.** (a) Voltage waveform of grid (b) Current waveform of grid

The waveforms of grid voltage and grid current are illustrated in Fig. 11 (a) & (b). Initially, the harmonics are occurred in the current waveform, which are eliminated after the time of $3 \times 10^{-4} s$ with the working of M5LC based PI. Thus, the waveform becomes pure sinusoidal.

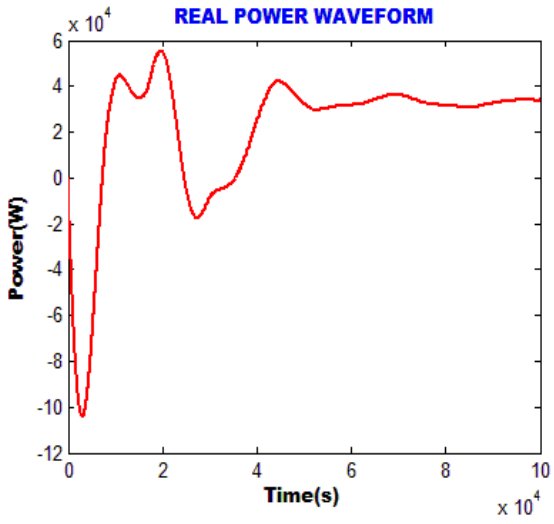


(a)

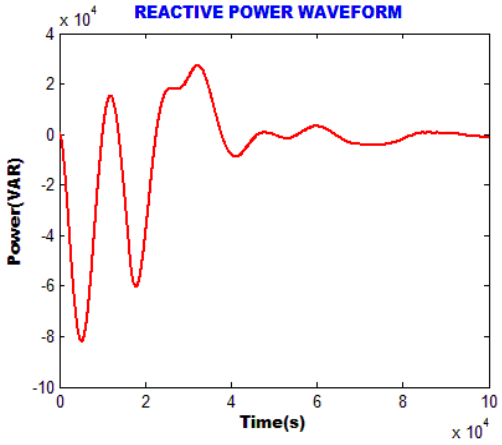


(b)

The waveforms of real and reactive powers are illustrated in Fig.12 (a) & (b). There are certain oscillations in the initial stage as shown in the waveforms, which are eliminated with the utilization of M5LC based PI. It is noted that, the compensation occurs after the time of $4 \times 10^{-4}\ s$.

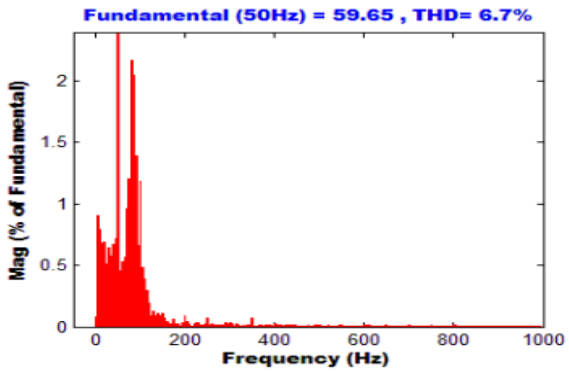


**Fig. 13**. THD of grid current using PI controller

The grid current THD using PI controller is illustrated in Fig. 13. The obtained THD of grid current is 6.7 % for PI controller.

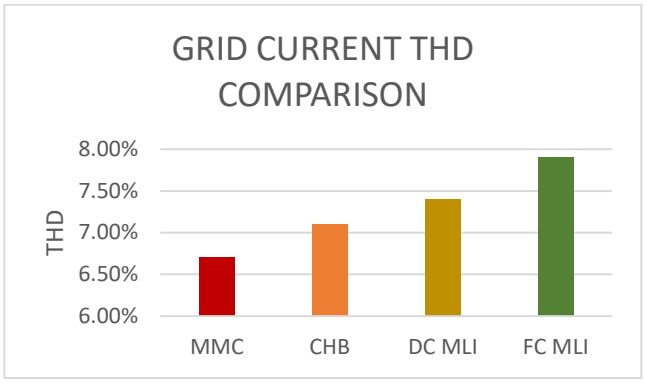


**Fig. 14.** Grid current THD comparative analysis

The comparative analysis of grid current THD is represented in Fig. 14. It is observed that the MMC based PI controller gives better performance with low grid current THD of 6.7 %, which is comparatively better than CHB, DC MLI and FC MLI.

## 5. Conclusion

The grid tied PV with M5LC is performed in this study, which has the beneficial factors like high modularity and easy scalability. The M5LC is used to enhance the voltage output of PV modules and the MCPWM technique is implemented for maintaining the converter's DC voltage as constant. The voltage output of M5LC is then supplied to grid via the VSI and the gating pulses of VSI are controlled through PI controller. The reference signal is produced by the PI controller and the produced reference signal is analogized with the carrier signals of MCPWM to control the VSI, which converts the DC into AC voltage. The grid synchronization is attained and the THD is minimized as 6.7 % with the help of PI controller. Thus, the proposed methodology is validated and its behavior is verified through MATLAB software.

## 6. References

[1]. N. Kumar, B. Singh and B. K. Panigrahi, "Framework of Gradient Descent Least Squares Regression-Based NN Structure for Power Quality Improvement in PV-Integrated Low-Voltage Weak Grid System", IEEE Transactions on Industrial Electronics, Vol. 66, No. 12, pp. 9724 – 9733, 2019.

[2]. V. N. Lal and S. N. Singh, "Control and Performance Analysis of a Single-Stage Utility-Scale Grid-Connected PV System", IEEE Systems Journal, Vol. 11, No. 3, pp. 1601 – 1611, 2017.

[3]. Avhankar, M. S. ., D. J. A. . Pawar, S. . Majalekar, and S. . Kedari. "Mobile Ad Hoc Network Routing Protocols – Using OPNET Simulator". International Journal on Recent and Innovation Trends in Computing and Communication, vol. 10, no. 1, Jan. 2022, pp. 01-07, doi:10.17762/ijritcc.v10i1.5513.

[4]. G. Petrone, G. Spagnuolo, R. Teodorescu, M. Veerachary and M. Vitelli, "Reliability Issues in Photovoltaic Power Processing Systems", IEEE

Transactions on Industrial Electronics, Vol. 55, No. 7, pp. 2569 – 2580, 2008.

[5]. Ghazaly, N. M. . (2022). Data Catalogue Approaches, Implementation and Adoption: A Study of Purpose of Data Catalogue. International Journal on Future Revolution in Computer Science &Amp; Communication Engineering, 8(1), 01–04. https://doi.org/10.17762/ijfrcsce.v8i1.2063

[6]. E. I. Amoiralis, M. A. Tsili and A. G. Kladas, "Power Transformer Economic Evaluation in Decentralized Electricity Markets", IEEE Transactions on Industrial Electronics, Vol. 59, No. 5, pp. 2329 – 2341, 2012.

[7]. A. Bag, B. Subudhi and P. K. Ray, "A combined reinforcement learning and sliding mode control scheme for grid integration of a PV system", CSEE Journal of Power and Energy Systems, Vol. 5, No. 4, pp. 498 – 506, 2019.

[8]. H. Liu, Y. Ji, L. Wang and P. Wheeler, "A Family of Improved Magnetically Coupled Impedance Network Boost DC–DC Converters", IEEE Transactions on Power Electronics, Vol. 33, No. 5, pp. 3697 – 3702, 2018.

[9]. M. Veerachary and P. Kumar, "Analysis and Design of Quasi-Z-Source Equivalent DC–DC Boost Converters", IEEE Transactions on Industry Applications, Vol. 56, No. 6, pp. 6642 – 6656, 2020.

[10]. Chawla, A. (2022). Phishing website analysis and detection using Machine Learning. International Journal of Intelligent Systems and Applications in Engineering, 10(1), 10–16. https://doi.org/10.18201/ijisae.2022.262

[11]. H. Wu, T. Mu, H. Ge and Y. Xing, "Full-Range Soft-Switching-Isolated Buck-Boost Converters With Integrated Interleaved Boost Converter and Phase-Shifted Control", IEEE Transactions on Power Electronics, Vol. 31, No. 2, pp. 987 – 999, 2016.

[12]. A. Anand and B. Singh, "Modified Dual Output Cuk Converter-Fed Switched Reluctance Motor Drive With Power Factor Correction", IEEE Transactions on Power Electronics, Vol. 34, No. 1, pp. 624 – 635, 2019.

[13]. P. K. Maroti, S. Padmanaban, J. B. Holm-Nielsen, M. S. Bhaskar, M. Meraj and A. Iqbal, " A New Structure of High Voltage Gain SEPIC Converter for Renewable Energy Applications" IEEE Access, Vol. 7, pp. 89857 – 89868, 2019.

[14]. M. Meraj, S. Rahman, A. Iqbal, L. Ben-Brahim and H. A. Abu-Rub, "Novel Level-Shifted PWM Technique for Equal Power Sharing Among Quasi-Z-Source Modules in Cascaded Multilevel Inverter", IEEE Transactions on Power Electronics, Vol. 36, No. 4, pp. 4766 – 4777, 2021.

[15]. M. S. A. Dahidah, G. Konstantinou and V. G. Agelidis, "A Review of Multilevel Selective Harmonic Elimination PWM: Formulations, Solving Algorithms, Implementation and Applications", IEEE Transactions on Power Electronics, Vol. 30, No. 8, pp. 4091 – 4106, 2015.

[16]. Ahmed Cherif Megri, Sameer Hamoush, Ismail Zayd Megri, Yao Yu. (2021). Advanced Manufacturing Online STEM Education Pipeline for Early-College and High School Students. Journal of Online Engineering Education, 12(2), 01–06. Retrieved from http://onlineengineeringeducation.com/index.php/joee/article/view/47

[17]. A. Moeini, H. Zhao and S. Wang, "Improve Control to Output Dynamic Response and Extend Modulation Index Range With Hybrid Selective Harmonic Current Mitigation-PWM and Phase-Shift PWM for Four-Quadrant Cascaded H-Bridge Converters", IEEE Transactions on Industrial Electronics, Vol. 64, No. 9, pp. 6854 – 6863, 2017.

[18]. S. K. Sahoo and T. Bhattacharya, "Phase-Shifted Carrier-Based Synchronized Sinusoidal PWM Techniques for a Cascaded H-Bridge Multilevel Inverter", IEEE Transactions on Power Electronics, Vol. 33, No. 1, pp. 513 – 524, 2018.

[19]. Y. Wang Orc, A. Aksoz, T. Geury, S. B. Ozturk, O. C. Kivanc and O. Hegazy, "A Review of Modular Multilevel Converters for Stationary Applications", MDPI Journal of Applied science, Vol. 10, No. 21, pp. 7719, 2020.